EUROPEAN ORGANIZATION FOR NUCLEAR RESEARCH

L3 Note 2086
May 16, 1997

Search for the Standard Model Higgs Boson at LEP2

L3 Higgs Group

J.Branson, A.Dominguez, I.Fisk, A.Kunin, L.Lugnier,
J.P.Martin, G.Raven, I.Vorobiev, J.Xu, B.Zhou

Abstract

A search for the Standard Model Higgs boson is performed using data collected with the L3 detector at LEP. The data sample corresponds to an integrated luminosity of 21.0 pb^{-1} at the centre of mass energies 161.3 GeV, 170.3 GeV and 172.3 GeV. No Higgs boson production is observed in the data, corresponding to the lower mass limit on the Standard Model Higgs boson $M_{\mathrm{H}} > 69.4$ GeV at 95% confidence level.

1 Introduction

At LEP2 energies the main production mechanism of the Standard Model Higgs boson is a 'higgs-strahlung' process:

$$e^+e^- \to Z^* \to HZ \tag{1}$$

The production cross-section of this process and Higgs boson decay branching fractions are the functions of its mass, which is an unconstrained parameter of the Standard Model [1]. The dominant final states of the reaction (1) for the Higgs mass in the range $60 < M_H < 80$ GeV are the following (the numbers correspond to the fractions of HZ system decays into a particular final state):

1)	$b\bar{b}q\bar{q}$	$(H \to b\bar{b},$	$Z \to q\bar{q})$	$\sim 60\%$
2)	$b\bar{b}\nu\bar{\nu}$	$(H \to b\bar{b},$	$Z \to \nu\bar{\nu})$	$\sim 17\%$
3)	$\tau^+\tau^- q\bar{q}$	$(H \to \tau^+\tau^-,$	$Z \to q\bar{q})$	$\sim 6\%$
4)	$b\bar{b}\tau^+\tau^-$	$(H \to b\bar{b},$	$Z \to \tau^+\tau^-)$	$\sim 3\%$
5)	$q\bar{q}e^+e^-$	$(H \to q\bar{q},$	$Z \to e^+e^-)$	$\sim 3\%$
6)	$q\bar{q}\mu^+\mu^-$	$(H \to q\bar{q},$	$Z \to \mu^+\mu^-)$	$\sim 3\%$

The most significant channel $e^+e^- \to HZ \to b\bar{b}q\bar{q}$ containing the 4-jet final state was not used in the LEP1 search [2] because of large QCD background. This background is considerably smaller at LEP2. In addition, use of the Silicon Micro-vertex Detector allows identification of the b-quark jets with high efficiency, greatly increasing the signal to background ratio for the Higgs boson searches.

At LEP1 with the centre of mass energy around the Z mass, $\sqrt{s} = 91.2$ GeV, the Standard Model Higgs boson search has reached the lower Higgs mass limit of 60.2 GeV [2]. In this note new results are presented using the data collected in the centre-of-mass energy range $161 \le \sqrt{s} \le 172$ GeV.

2 Data and Monte Carlo Samples

The data used for the analysis were collected in 1996 by the L3 detector at LEP. The integrated luminosity is 10.8, 1.0 and 9.2 pb^{-1} collected at the centre-of-mass energies $\sqrt{s} = 161.3$, 170.3 and 172.3 GeV respectively.

The L3 detector is described in reference [3]. Briefly, the e^+e^- collision point is surrounded by a precision silicon vertex detector, a time-expansion tracking chamber (TEC), a high resolution electromagnetic calorimeter (ECAL), a cylindrical shell of scintillation counters, a hadron calorimeter (HCAL), a muon spectrometer and a very forward calorimeter used for the luminosity measurements. The detector is installed in a large solenoidal magnet providing a 0.5 T field.

In order to study the production and decay of the Higgs boson, and to determine the acceptance of the detector and the efficiencies of the selections, Monte Carlo simulations of different processes has been performed. Higgs boson production was generated in the $Hq\bar{q}$, $H\nu\bar{\nu}$, He^+e^-, $H\mu^+\mu^-$ and $H\tau^+\tau^-$ and $\tau^+\tau^-Z$ channels in the Higgs mass range from 50 to 80 GeV. In this mass range the Higgs boson decays predominantly into a $b\bar{b}$ pair, although the branching ratios into $c\bar{c}$ and $\tau^+\tau^-$ are not negligible. The Monte Carlo event generator program includes initial state photon radiation and final state radiation of photons from leptons and gluons from quarks. For each channel different background sources have also been simulated.

The number of simulated background events are about 100 times the statistics of the collected data samples.

The L3 detector response is simulated using the GEANT 3.15 program [4], which takes into account the effects of energy loss multiple scattering and showering in the detector. The GHEISHA program [5] is used to simulate hadronic interactions in the detector.

3 Analysis Technique

The search for Standard Model Higgs boson at LEP2 comprises four independent topological selections of the final states produced in the process $e^+e^- \rightarrow HZ$: $Hq\bar{q}$, $H\nu\bar{\nu}$, $\tau^+\tau^- q\bar{q}$ and $H\ell^+\ell^-$. The optimal separation between the signal and the background in every channel after a tight preselection is achieved using a neural network technique [6]. The main goal of the preselection is to bring down the number of expected background events to 10-30, while keeping the signal efficiency high - of the order 70%. This provides optimal starting point for the neural network implementation. The same type of feed-forward neural network with one layer of input nodes, one layer of hidden nodes and one output node is used for all the final state channels. The number of hidden nodes used in the analysis is usually two times the number of input variables. The input information to the neural network consists of topological variables similar to those used in the Higgs boson search at LEP1 [2] and a B-tagging variable which characterises b-quark content of an event.

The definition of the B-tag variable, B_{tag} is based upon the lifetime information. This variable is constructed using decay length of all the tracks. The track decay length, L, is defined as a distance from the primary event vertex to the intersection point of the track with the axis of the closest jet. The probability that a track originates from the primary vertex, $P(L/\sigma_L)$, is obtained from the control sample of tracks with negative decay length. The probability that all tracks in an event come from the primary vertex is calculated in the following way:

$$P_N = \frac{\Pi}{2^N} \sum_{i=0}^{N-1} \sum_{j=i+1}^{N} \left(\begin{array}{c} N \\ j \end{array} \right) \frac{(-\log \Pi)^i}{i!} \,, \qquad \Pi = \prod_{j=1}^{N_+} P_j(L/\sigma_L) \tag{2}$$

where N_+ is the number of tracks with positive decay length. By construction this variable is flat for events without lifetime, whereas events containing tracks originating from the secondary vertices show up as a peak at zero. The B_{tag} variable is then defined: $B_{\text{tag}} = -\log_{10} P_N$. The spectrum of this variable for the sample of $e^+e^- \rightarrow Z \rightarrow q\bar{q}$ events is presented in Figure 1a. Figure 1b shows the efficiency for $Z \rightarrow b\bar{b}$ events and the purity of the sample as functions of the cut on this variable.

Extensive studies of the systematic errors associated to the use of the neural network have been carried out to verify its performance. First, to determine the signal efficiency and background contamination in the signal-sensitive regions (i.e. high values of the neural net output) the Monte Carlo samples were used statistically independent from those used for the neural net training. Second the systematic errors in the input variables (usually associated to the energy scale uncertainties, noise in the detector, and performance of the tracking chamber) were studied by changing the neural net input variables according to these uncertainties. The correspondent efficiency change does not exceed 6% (for the $Hq\bar{q}$ and $H\nu\bar{\nu}$ analyses), whereas the average shift is of the order 2%. The propagation of these uncertainties to the final result causes the 50 MeV decrease of the final mass limit.

4 Event Selection

4.1 The $\mathrm{Hq\bar{q}}$ channel

The $\mathrm{Hq\bar{q}}$, $\mathrm{H} \rightarrow \mathrm{b\bar{b}}$ channel has the largest branching fraction ($\sim 60\%$) for the M_{H} range accessible at LEP2. The signature of these events is four jets with two of them containing b-quarks. They are characterised by high multiplicity of tracks and calorimetric energy clusters. The invariant mass of one jet pair is consistent with the Z mass.

The main background comes from $\mathrm{q\bar{q}}$ events with hard gluon radiation and from the $\mathrm{W^+W^-}$ hadronic decays. The event selection proceeds in three steps. First, hardonic events with at least 5 tracks and 15 calorimetric clusters are selected requiring the visible energy, E_{vis} of the event to greater than $0.5\sqrt{s}$ and smaller than $2.0\sqrt{s}$. The event energy imbalance must not exceed 50% of the visible energy.

Then events containing at least four jets are selected. Jet are reconstructed using JADE clustering scheme with the parameter $Y_{\mathrm{cut}} = 0.02$. Events containing more than four jets are forced to have exactly four jets using the DURHAM algorithm [7]. The energy and momentum conservation constraints are applied in the kinematic fit to improve the invariant mass resolution of jet pairs. The expectations from the Standard Model processes of 23.1 events at $\sqrt{s} = 161$ GeV and 36.6 four jet events at $\sqrt{s} = 172$ GeV are in a good agreement with the actual observations of 23 and 38 events respectively. The signal selection efficiency is estimated to be 58.6% at $\sqrt{s} = 161$ GeV and 55.5% at $\sqrt{s} = 172$ GeV

Finally the neural network is constructed to further discriminate between the signal and the background. Fourteen variables are used as an input to the network. These variables are: the visible energy; the missing energy; the direction of the missing energy; the maximum photon energy; the energies deposited in the electromagnetic and in the hadron calorimeters; the event thrust; the event centrality, which is defined as sum of the jet transverse energies divided by sum of the jet energies; the number of charged tracks; the number of calorimeter energy clusters; minimum di-jet mass; minimum sum of di-jet mass; number of charged tracks with long lifetime information; the B_{tag} variable. Figure 2 shows data and Monte Carlo comparison for the most important variables used as the neural network input. The distributions of the network output for the $\sqrt{s} = 161$ GeV and 172 GeV data samples are presented in Figure 3 along with the background expectations and Monte Carlo predictions for 70 GeV Higgs boson signal.

The control data sample of four-jet events was used to verify the validity of the efficiency and the background estimates using neural network analysis. $\mathrm{W^+W^-}$ pair decays into four jet final state is similar to the $\mathrm{Hq\bar{q}}$ events except that Higgs bosons predominantly decay into $b\bar{b}$ pairs, while W decays into b-jets are highly suppressed. The same neural network as the one used for the Higgs boson search is trained to identify $\mathrm{W^+W^-}$ pairs. The cross-section of $\mathrm{W^+W^-}$ pair production with the consecutive decay into four jets is measured to be $5.53^{+1.23}_{-1.06}$ pb at $\sqrt{s} = 172$ GeV using a binned likelihood fit to a data distribution presented in Figure 4. This measurement is consistent with the Standard Model expectations as well as it agrees with the recent L3 measurement using a dedicated analysis [8].

4.2 The $\mathrm{H}\nu\bar{\nu}$ channel

The selection of candidates for the process $\mathrm{e^+e^-} \rightarrow \mathrm{H}\nu\bar{\nu}$, $\mathrm{H} \rightarrow \mathrm{b\bar{b}}$ is based on the following requirements: two acoplanar hadronic jets, no leptons, large missing transverse energy and secondary vertices due to B-hadron decays.

High multiplicity hadronic events with more than two charged tracks and more than ten calorimetric energy clusters are selected. The energy in the forward luminosity calorimeters is required to be smaller than 10 GeV. All energy clusters in the event are combined to form two hadronic jets using the DURHAM algorithm. The invariant mass of these jets, M_{VIS}, is required to exceed 30 GeV. These cuts reduce contributions from the pure leptonic final states $\mathrm{e^+e^-} \to \mathrm{e^+e^-}(\gamma)$, $\mu^+\mu^-(\gamma)$, $\tau^+\tau^-(\gamma)$ and two-photon interactions $\mathrm{e^+e^-} \to \mathrm{e^+e^-q\bar{q}}$ while keeping a significant fraction of hadronic events from $\mathrm{e^+e^-} \to \mathrm{Z}(\gamma)$ and $\mathrm{e^+e^-} \to \mathrm{W^+W^-}$. It is reduced by requiring $M_{\mathrm{VIS}} < 90$ GeV (see Figure 5a).

To reject further events from the two fermion production process $\mathrm{e^+e^-} \to \mathrm{q\bar{q}}(\gamma)$ the transverse missing energy, $E_\perp$, is required to exceed 6 GeV. The missing momentum vector must be at least 0.32 rad away from the beam axis and the energy in the 0.44 rad sector along its direction, $E^{25^o}_{\mathrm{mis}}$, must be below 25 GeV (see Figure 5b). Events containing identified leptons with energy greater than 15 GeV are rejected in order to suppress the remaining background from $\mathrm{e^+e^-} \to \mathrm{W^+W^-}$ where one of the W bosons decays into leptons. In addition the B-tagging variable, B_{tag}, is required to be greater than zero (see Figure 5c).

Nine candidate events are selected in the $\sqrt{s} = 161$ GeV data sample and 15 in the $\sqrt{s} = 172$ GeV data sample consistent with the background expectation of 7.0 and 10.6 respectively. The signal efficiency for 70 GeV Higgs Boson is found to be $(65 \pm 2)\%$ at $\sqrt{s} = 161$ GeV and $(77 \pm 1)\%$ at $\sqrt{s} = 172$ GeV.

Neural network is then used to construct a discriminant variable that further separates the signal from the background. Eight variables are used as an input to the net: $E_\perp$, M_{VIS}, $\max(M_{j_1}, M_{j_2})$, $E^{25^o}_{\mathrm{mis}}$, $E^{40^o}_{\mathrm{mis}}$, M_{MIS}, B_{tag} and θ_{123}. The last one correspond to the stereo angle defined by the directions of three jets which are formed for every event using the DURHAM algorithm (shown in Figure 5d). The neural net output spectra for the $\sqrt{s} = 161$ GeV and 172 GeV data samples are shown in Figure 6. These spectra, along with those from other channels, are used to extract a signal likelihood function.

The systematics related to the use of the neural network was studied by changing the energy calibration by $\pm 3\%$ what corresponds to a maximal possible uncertainty in the calibration procedure, extra smearing of $E^{25^o}_{\mathrm{mis}}$ and $E^{40^o}_{\mathrm{mis}}$ variables according to the noise studies in the beam-gate the events. The maximal deviation of 6% is observed, whereas the average shift is estimated not to exceed 1-2%. The systematics of $\pm 2\%$ was assigned due to the use of B_{tag} variable from the comparison of data and Monte Carlo spectra of this variable for $\mathrm{Z} \to \mathrm{q\bar{q}}$ events. The account of other Higgs boson decays: $\mathrm{H} \to \mathrm{c\bar{c}}$ and $\mathrm{H} \to \mathrm{gg}$, results in the 2% increase of the efficiency for the $\mathrm{H} \to \mathrm{b\bar{b}}$ channel.

As a cross-check of the neural network performance production cross-section of the process $\mathrm{e^+e^-} \to \mathrm{We}\nu$, $\mathrm{W} \to \mathrm{qq'}$ was measured at $\sqrt{s} = 172$ GeV. The same neural network as the one used for the Higgs boson search is trained to identify $\mathrm{We}\nu$ events. The result, $\sigma(\mathrm{e^+e^-} \to \mathrm{We}\nu) = 0.78^{+1.13}_{-0.66}$ pb, is compatible with that obtained with the dedicated analysis [9].

4.3 The $\mathrm{He^+e^-}$ and $\mathrm{H}\mu^+\mu^-$ channels

The specific signature of $\mathrm{He^+e^-}$ and $\mathrm{H}\mu^+\mu^-$ is a pair of two high energy electrons or muons with the invariant mass close to M_{Z} accompanied by two hadronic jets.

High multiplicity hadronic events with more than four tracks and more than twenty calorimetric energy clusters and two high energy leptons, $E_{\mathrm{lept}} > 15$ GeV, are selected. The angle between the leptons is required to exceed 1.6 rad and the invariant mass of the hadronic system, M_{had}, has to be greater 25 GeV.

For the $\mathrm{H}\mu^+\mu^-$ selection both muons are identified as tracks in the Muon Chamber system. The $\mathrm{He}^+\mathrm{e}^-$ selection requires one electron to be identified as a shower having an electromagnetic shape and a track pointing to it, while the only requirement on another is that it has at least 15 GeV of energy deposition in the calorimeters. This selection allows to keep acceptance high for $\mathrm{He}^+\mathrm{e}^-$ events where one of the electrons produces a shower in the vicinity of non-homogenius regions in the detector.

Three $\mathrm{He}^+\mathrm{e}^-$ candidate events are selected in the $\sqrt{s} = 161$ GeV data sample and three in the $\sqrt{s} = 172$ GeV data sample consistent with the background expectation of 2.3 and 3.6 events respectively. The signal efficiency for 70 GeV Higgs Boson is found to be $(67.9 \pm 2)\%$ at $\sqrt{s} = 161$ GeV and $(76.2 \pm 1)\%$ at $\sqrt{s} = 172$ GeV. Invariant mass of the selected electron pairs at $\sqrt{s} = 172$ GeV is presented in Figure 7a.

One $\mathrm{H}\mu^+\mu^-$ candidate events is selected in the $\sqrt{s} = 161$ GeV data sample and three in the $\sqrt{s} = 172$ GeV data sample consistent with the background expectation of 2.2 and 2.8 events respectively. The signal efficiency for 70 GeV Higgs Boson is found to be $(46.0 \pm 2)\%$ at $\sqrt{s} = 161$ GeV and $(50.1 \pm 1)\%$ at $\sqrt{s} = 172$ GeV. Invariant mass of the selected muon pairs at $\sqrt{s} = 172$ GeV is presented in Figure 8a.

Neural network is then used to construct a discriminant variable that further separates the signal from the background. Five variables are used as an input to the net: E^1_{lept}, E^1_{lept}, M_{12}, M_{had} and α_{12}. The last one corresponds to the angle between the leptons. The neural net output spectrum for the $\mathrm{He}^+\mathrm{e}^-$ and $\mathrm{H}\mu^+\mu^-$ channels at $\sqrt{s} = 172$ GeV are shown in Figures 7b and 8b respectively.

4.4 The $\tau^+\tau^-\mathrm{q\bar{q}}$ Final States

The signatures of $\mathrm{Hq\bar{q}}$, $\mathrm{H} \rightarrow \tau^+\tau^-$ and $\mathrm{H}\tau^+\tau^-$, $\mathrm{H} \rightarrow \mathrm{b\bar{b}}$ events is similar to that of $\mathrm{H}\ell^+\ell^-$ channel except the tau leptons are identified as a pair of low multiplicity jets.

High multiplicity hadronic events with more than four tracks and more than twenty calorimetric energy clusters and two high energy tau jets ($E_{\mathrm{lept}} > 5$ GeV) are selected. The energy in the 20^o cone around lepton must be less than half of its energy to insure separation of leptons from jets. The opening angle between the τ-leptons and the angle between the hadronic jets are both required to be greater than 1.5 rad. The invariant mass of the tau jets, $M_{\tau\tau}$, and the hadronic system complimentary to the tau-jets, M_{had}, are required to be consistent with M_{Z} and M_{H}, respectively and depending on the search channel, within the measurement errors.

After these cuts 5 events are selected for the channel $\mathrm{HZ} \rightarrow \tau^+\tau^-\mathrm{q\bar{q}}$ at 161 GeV with 5.7 expected background events (efficiency of selection is 29.7%), and at 172 GeV 6 events are selected with 5.9 events expected (efficiency of selection is 28.9%). Invariant mass of the hadronic system for the selected events at $\sqrt{s} = 172$ GeV is presented in Figure 9a together with the background expectations. For $\mathrm{HZ} \rightarrow \mathrm{b\bar{b}}\tau^+\tau^-$ these numbers are 3 and 4.2 (efficiency is 31.7%) at 161 GeV and 5 and 5.0 (efficiency is 30.4%) at 172 GeV.

Neural network is then used to construct a discriminant variable that further separates the signal from the background. The input variables are: energy of each lepton, angle between two leptons, their mass, energy in cones around leptons, energy of each jet, their mass, thrust of two jets, number of smallest resolvable clusters in the event. In addition for the $\mathrm{H}\tau^+\tau^-$, $\mathrm{H} \rightarrow \mathrm{b\bar{b}}$ channel the B_{tag} variable is used. The spectrum of the output of the neural network variable for the $\mathrm{HZ} \rightarrow \tau^+\tau^-\mathrm{q\bar{q}}$ channel is shown in Figure 9b.

5 Systematic uncertainties

Several sources of the systematic effects are considered in the present analysis. The procedure, adopted in this note to account for the systematics, is following: if there exist a systematic difference between data and Monte Carlo estimates, the corresponding correction is applied to the respective signal efficiency or background contamination estimates followed by the smearing of the final signal likelihood function by the amount of the uncertainty in the correction factor.

The integrated luminosity, which is measured to be $10.90\mathrm{pb}^{-1}$, $1.00\mathrm{pb}^{-1}$ and $9.25\mathrm{pb}^{-1}$ at the centre-of-mass energies $\sqrt{s} = 161.3$, 170.3 and 172.3 GeV respectively has been corrected to account for TEC and HCAL inefficiencies. The integrated luminosity when TEC was off is estimated to be $0.084\mathrm{pb}^{-1}$ in the 96a running period and $0.029\mathrm{pb}^{-1}$ in the 96b. The corresponding numbers for the Hadron Calorimeter endcaps are $0.003\mathrm{pb}^{-1}$ and $0.057\mathrm{pb}^{-1}$ respectively. This luminosity was not used to calculate the expected number of signal and background events. No other detector inefficiencies were observed.

The TEC efficiency estimate performed using real detector simulation is found to be too conservative: from 2.5% to 4.0% of all Monte Carlo events have no tracks at all - the effect which is not present in the data. Therefore both signal efficiency and background rate are increased by 3% and 1% systematic uncertainty is assigned to this correction.

No other significant systematic effects are identified in the estimates of the background rates. Pure statistical errors, which can be as large as 30%, dominate in the signal sensitive regions. They are accounted for in the derivation of the final limit.

Effects of limited statistics may constitute one of the major sources of the uncertainties in the final result. These effects arise when a data event pops up in a bin with no background events. In these circumstances the difference in the final mass limit calculated with the background shape directly from the low statistics Monte Carlo (on average 100 times the data statistics) and the shape smoothed in advance may result in a mass limit changing by $0.4 - 0.5$ GeV. This situation does not happen for the given data pattern observed in this analysis, and therefore this systematic error is neglected (but it deserves more studies in future).

The contribution of Higgs boson decays into $\mathrm{c\bar{c}}$ and gg final states is not accounted for in the $\mathrm{Hq\bar{q}}$ analysis. Using the results of $\mathrm{H}\nu\bar{\nu}$ analysis related to these decays, the net effect is estimated to be $(2.0 \pm 0.5)\%$ increase in the $\mathrm{b\bar{b}q\bar{q}}$ selection efficiency.

6 Results

The likelihood as a function of the number of expected signal events is determined from the distributions of the neural net output for all the channels and all centre-of-mass energies (the corresponding distributions for $\mathrm{Hq\bar{q}}$, $\mathrm{H}\nu\bar{\nu}$, $\mathrm{He^+e^-}$, $\mathrm{H}\mu^+\mu^-$ and $\tau^+\tau^-\mathrm{q\bar{q}}$ channels are presented in Figures 3 and 6, 7b, 8b and 9b respectively) using Poisson statistics for the number of observed data events, $N_{i,k}$:

$$\mathcal{L}(\mu_{\mathrm{H}}) = \prod_{k=1}^{n_{\mathrm{ch}}} \prod_{i=1}^{n_{\mathrm{bn}}^{k}} \frac{e^{-(\mu_{\mathrm{H},i,k}+\mu_{\mathrm{b},i,k})}(\mu_{\mathrm{H},i,k}+\mu_{\mathrm{b},i,k})^{N_{i,k}}}{N_{i,k}!}, \tag{3}$$

where the product is taken over all search channels ($k = (1, n_{\mathrm{ch}})$) and all bins ($i = (1, n_{\mathrm{bn}})$). The background shapes and normalisations are fixed to the Monte Carlo prediction ($\mu_{\mathrm{b},i,k}$). The individual signal expectations, ($\mu_{\mathrm{H},i,k}$), are proportional to the total number of signal events, μ_{H}, corresponding branching fractions, $\mathcal{B}_k$, and efficiencies, $\epsilon_{i,k}$. The likelihood function for the

70 GeV Higgs boson is presented in Figure 10a. The likelihood value for $\mu_{\mathrm{H}} = 0$ represents consistency of the data with the background expectations; the larger $\mathcal{L}(0)$ values correspond to better agreement. This is quantified by performing 10000 Monte Carlo experiments. Each experiment generates "observations" using the background expectations and Poisson statistics. The simulated $\mathcal{L}(0)$ spectrum is shown in Figure 10b, together with the result of our experiment. The probability of having the likelihood value equal or less then that actually observed is estimated to be 71% using Monte Carlo simulation of possible data patterns for the given background spectra. Given the consistency of the data with the background expectations, it is concluded that no indication for the Higgs boson production is observed.

Another way of looking at it is to order all the neural network output bins for all the channels under investigation according to signal to background ratio. This is illustrated in Figure 11a, where this ordering is presented keeping in addition the background contamination 0.1 event/bin.

The signal probability density function is then constructed using Bayesian statistics [10,11]:

$$\mathrm{P}(\mu_{\mathrm{H}})\mathrm{d}\mu_{\mathrm{H}} = \frac{\mathcal{L}(\mu_{\mathrm{H}})\mathrm{d}\mu_{\mathrm{H}}}{\int \mathcal{L}(\mu_{\mathrm{H}})\mathrm{d}\mu_{\mathrm{H}}} \tag{4}$$

in order to derive 95% confidence level limit on the number of signal events. For the 70 GeV Higgs boson the integrated probability (confidence level) that the production cross-section exceeds the Standard Model prediction is calculated to be 7.6%. The spectrum of the confidence levels obtained performing Monte Carlo experiments as described above is shown in Figure 11b. The average expected confidence level, defined as the one having 50% probability, is calculated to be 12.5%. The probability to have a confidence level equal or smaller than one actually observed is estimated to be 29.2%.

The statistical and systematic errors on the background rate and signal efficiency are accounted for by reweighting the probability density function (4) according to the estimated uncertainties. In addition the correction is applied to the probability calculated using Equation 4 such that the corrected confidence level corresponds to a signal fail rate in the classical statistics approach [12]. This increases the lower mass limit by 0.3 GeV. The corrected 95% confidence level for the number of expected signal events as a function of the Higgs boson mass is shown in Figure 12 together with the Standard Model predictions for the number of expected Higgs events. The crossing point is at 69.4 GeV - the Higgs boson mass limit resulting from this analysis. The average expected limit, defined as the one having 50% probability, is estimated to be 68.1 GeV using Monte Carlo simulation. Another estimate based on the average confidence level over all Monte Carlo experiments gives 67.0 GeV.

References

[1] S.L.Glashow, Nucl.Phys. **22** (1961) 579;
S.Weinberg, Phys.Rev.Lett. **19** (1967) 1264;
A.Salam, "Elementary Particle Theory", Ed. N. Svartholm, Stockholm, "Almquist and Wiksell", (1968), 367.

[2] M. Acciarri *et al.*, L3 Collaboration, Phys.Lett. **B 385** (1996) 454.

[3] L3 Collaboration, B.Adeva *et al.*, Nucl.Instr.Meth. **A289** (1990) 35; J.A.Bakken *et al.*, Nucl.Instr.Meth. **A275** (1989) 81; O.Adriani *et al.*, Nucl.Instr.Meth. **A302** (1991) 53; B.Adeva *et al.*, Nucl.Instr.Meth. **A323** (1992) 109; K.Deiters *et al.*, Nucl.Instr.Meth. **A323** (1992) 162; B.Acciari *et al.*, Nucl.Instr.Meth. **A351** (1994) 300; A.Adam *et al.*, Nucl.Instr.Meth. **A383** (1996) 342.

[4] R.Brun *et al.*, preprint CERN DD/EE/84-1 (Revised 1987).

[5] H.Fesefeldt, RWTH Aachen Report PITHA 85/02 (1985).

[6] L. Lonnblad, C. Peterson and T. Rognvaldsson, Nucl. Phys. B349(1991)675.

[7] S.Catani *et al.*, Phys.Lett. **B 263** (1991) 491;
S.Bethke *et al.*, Nucl.Phys. **B 370** (1992) 310.

[8] M. Acciarri *et al.*, L3 Collaboration, "$\mathrm{W}^+\mathrm{W}^-$ *pair production at* $\sqrt{s}$ = 172 GeV.", in preparation.

[9] M. Acciarri *et al.*, L3 Collaboration, preprint CERN-PPE/97-28, submitted to Phys.Lett. B.

[10] R.M.Barnett *et al.*, Particle Data Group Phys.Rev. **D54** (1996) 1.

[11] O.Helen, Nucl.Instr.Meth. **A257** (1987) 346.

[12] J.F.Grivaz and F.LeDiberder, Nucl.Instr.Meth. **A333** (1993) 320.

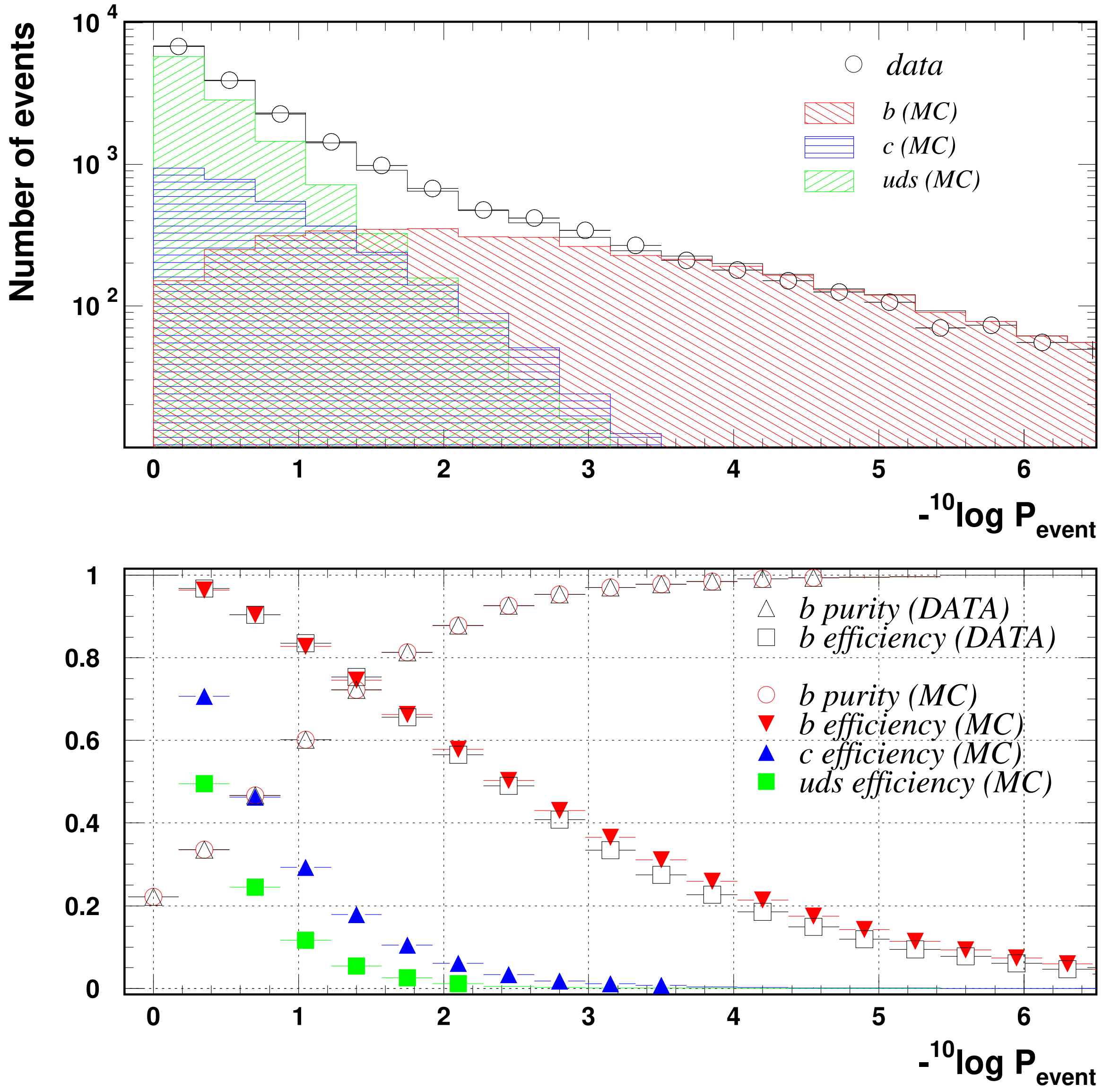

Figure 1: The spectrum of the $B_{\rm tag}$ variable for the sample of $\mathrm{Z} \to \mathrm{q\bar{q}}$ events (a). The purity of the sample and the efficiency for $\mathrm{Z} \to \mathrm{b\bar{b}}$ events (b) are presented as functions of the cut on the $B_{\rm tag}$ variable.

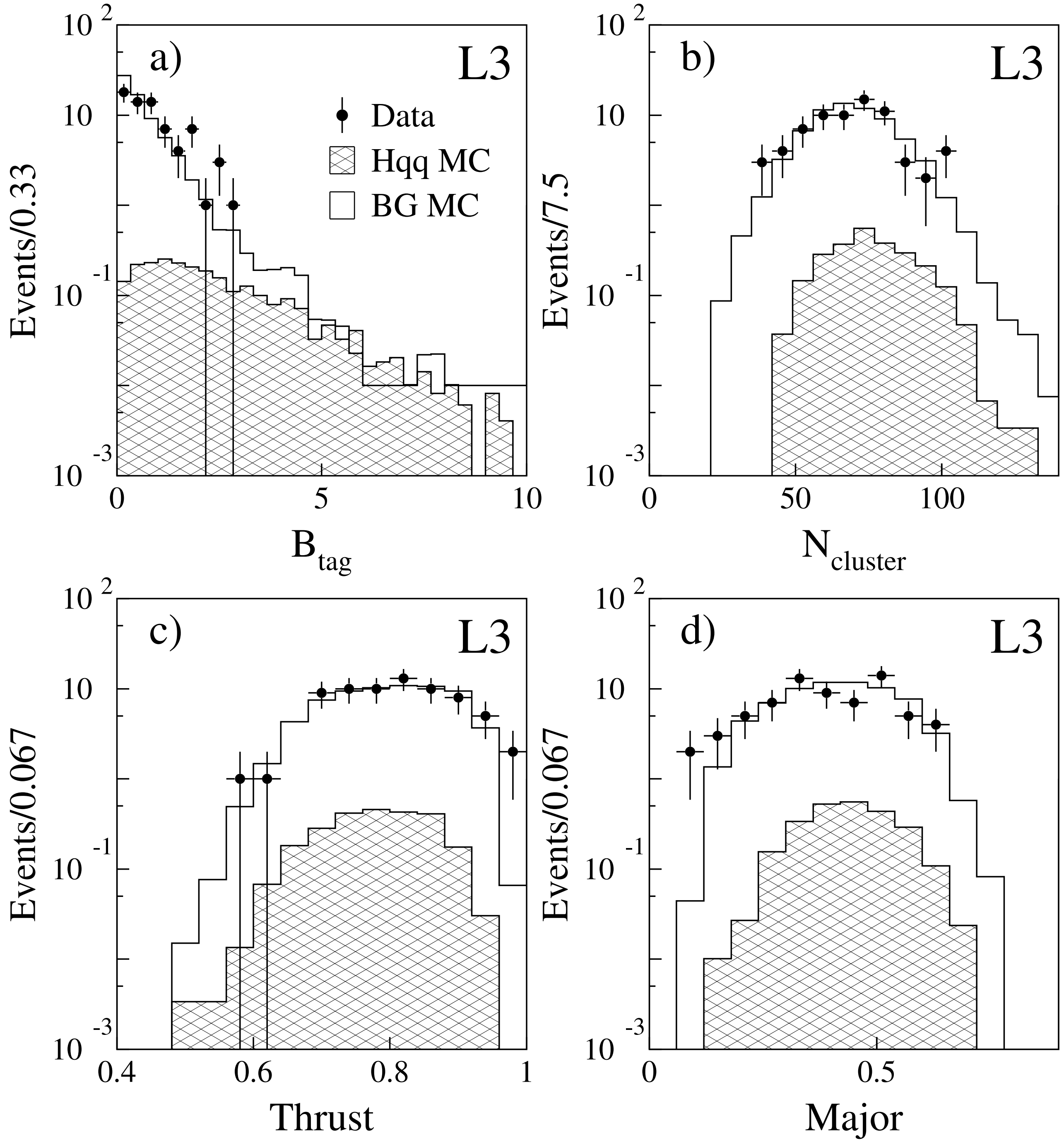

Figure 2: The most important variables used as the neural network input for the H$q\bar{q}$ analysis: (a) $B_{\rm tag}$ variable; (b) number of calorimetric clusters; (c) event thrust, (d) event major.

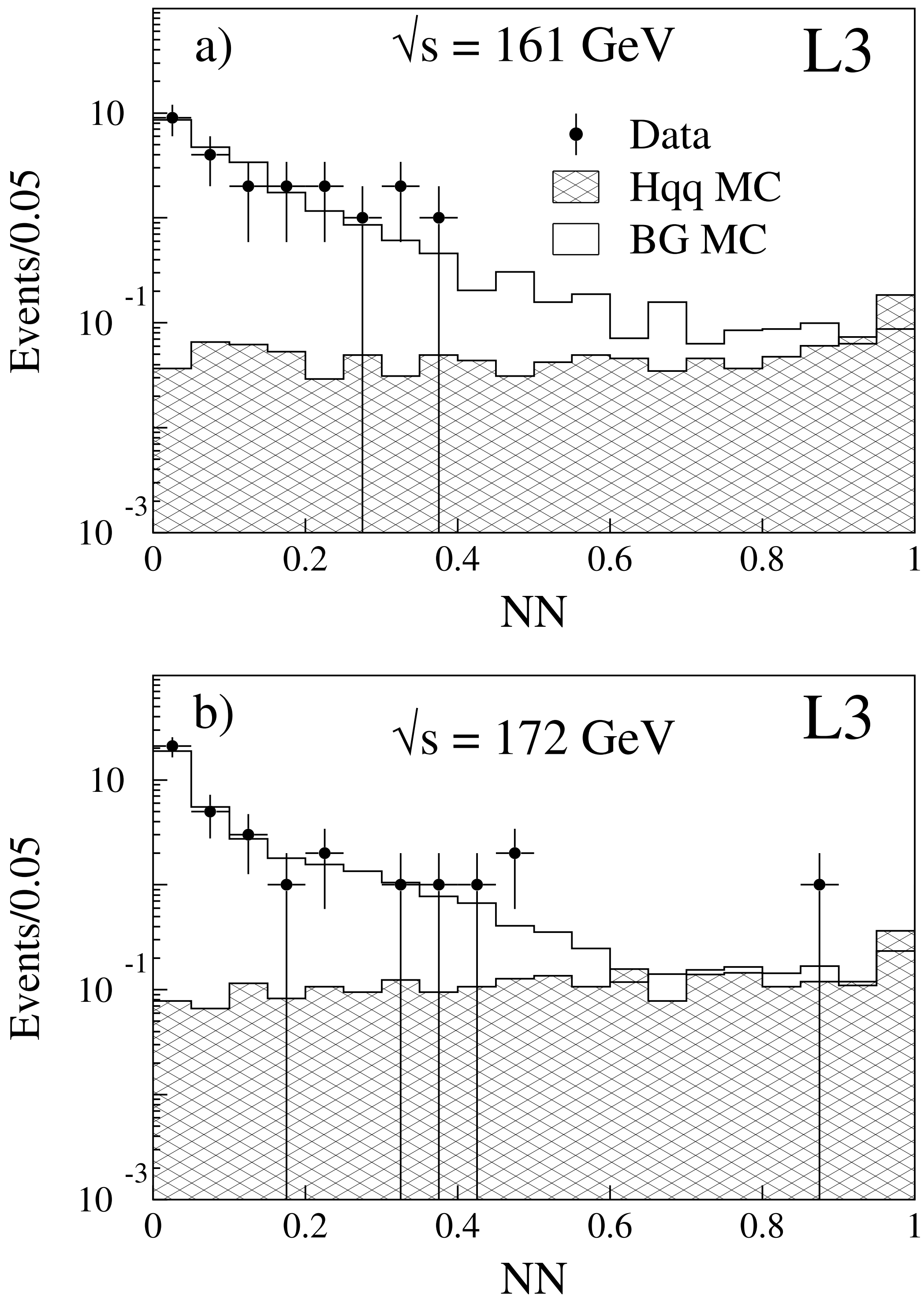

Figure 3: Final Hq$\bar{q}$ neural network output spectra for the $\sqrt{s}$ = 161 GeV and 172 GeV data samples. The hatched histograms correspond to the 70 GeV Higgs boson signal normalised to the Standard Model cross-section.

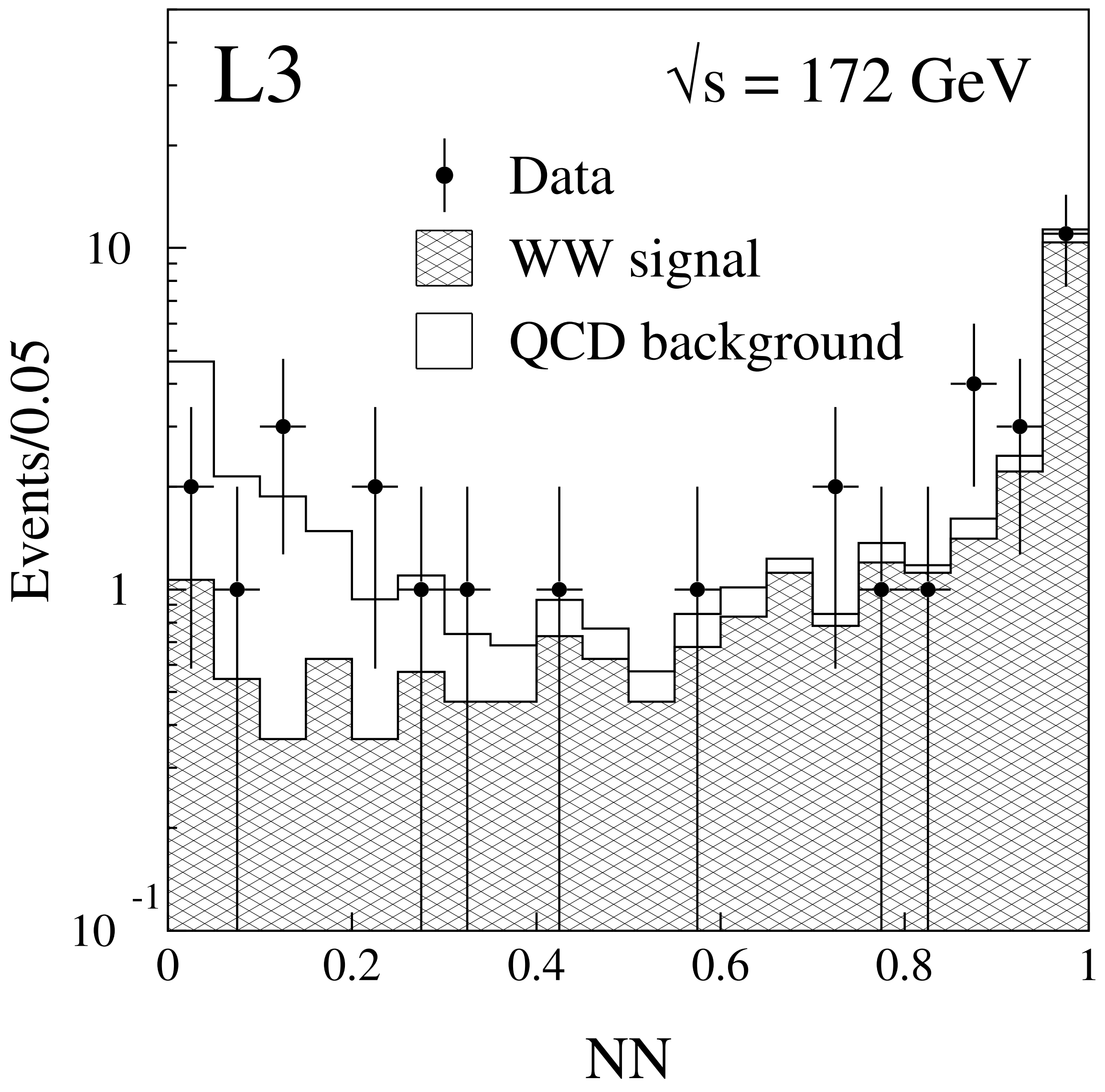

Figure 4: Neural network output spectra for the $W^+W^- \rightarrow q\bar{q}$ cross-section fit at $\sqrt{s}$ = 172 GeV. The hatched histogram represents the fitted $W^+W^- \rightarrow q\bar{q}$ contribution.

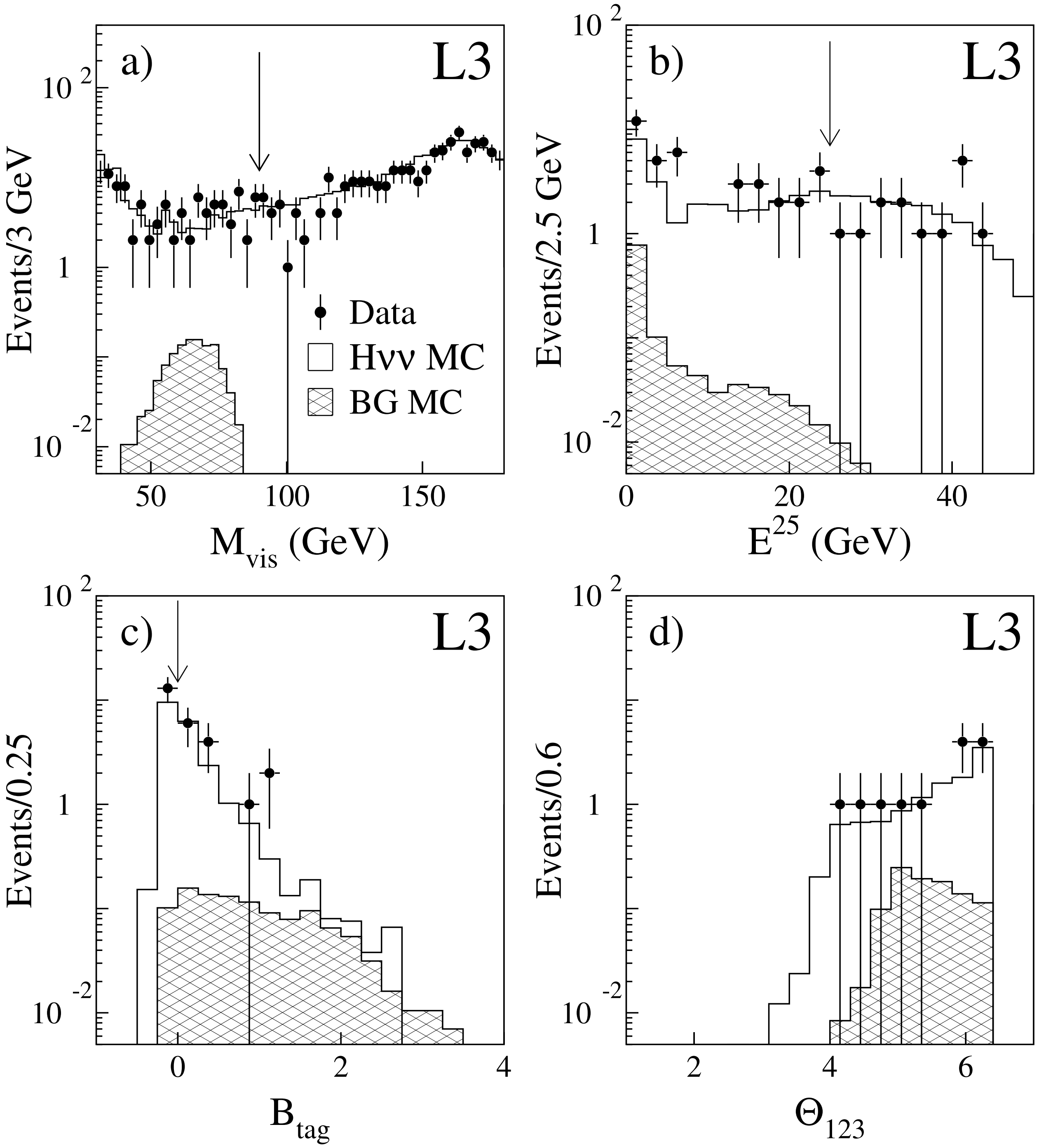

Figure 5: The most important variables used as the neural network input for the $\mathrm{H}\nu\bar{\nu}$ analysis: (a) the invariant mass of the two jets, M_{VIS}; (b) the energy in the 25^o sector around the missing energy direction, $E^{25^o}_{\mathrm{mis}}$; (c) B_{tag} variable; (d) the opening angle between the two jets, θ_{123}.

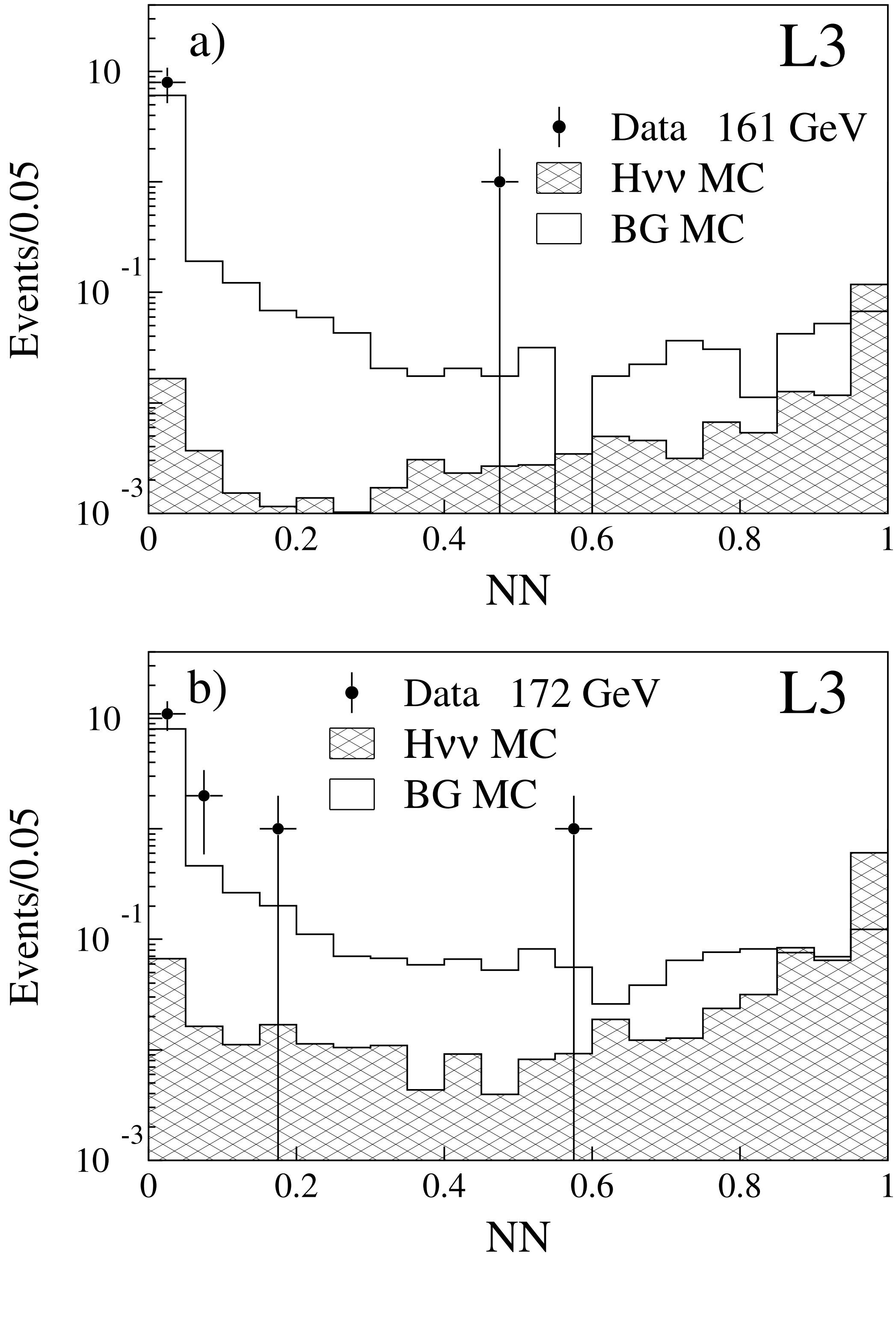

Figure 6: Final $H\nu\bar{\nu}$ neural network output spectra for the $\sqrt{s} = 161$ GeV and 172 GeV data samples. The hatched histograms correspond to the 70 GeV Higgs boson signal normalised to the Standard Model cross-section.

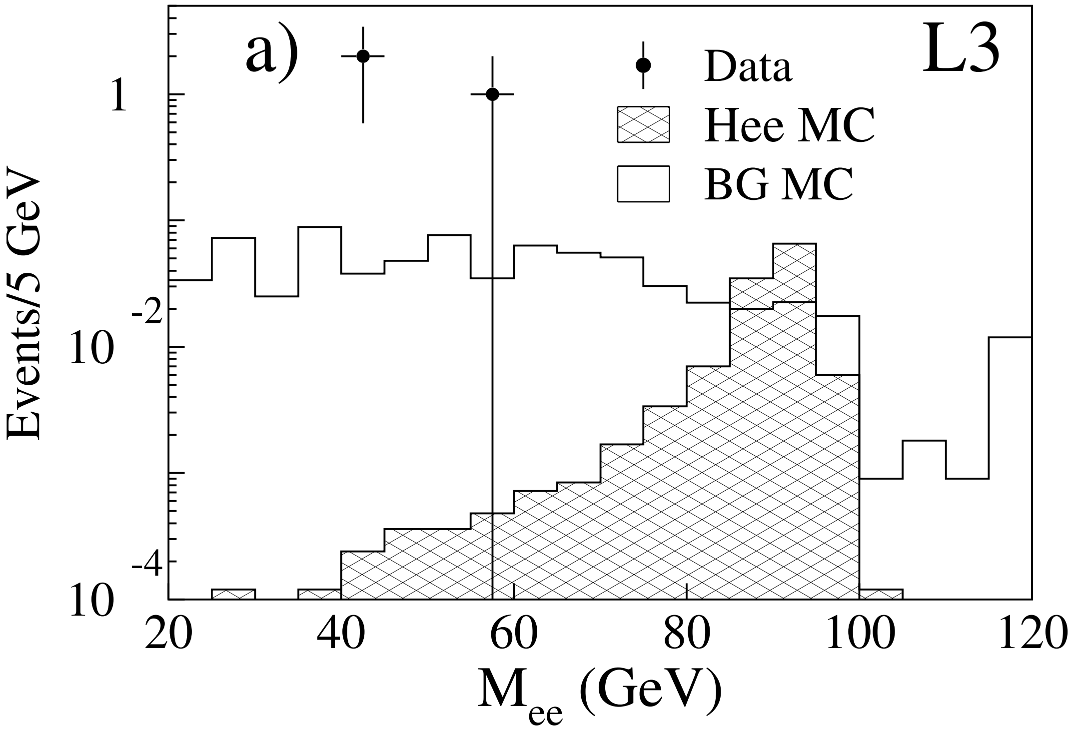

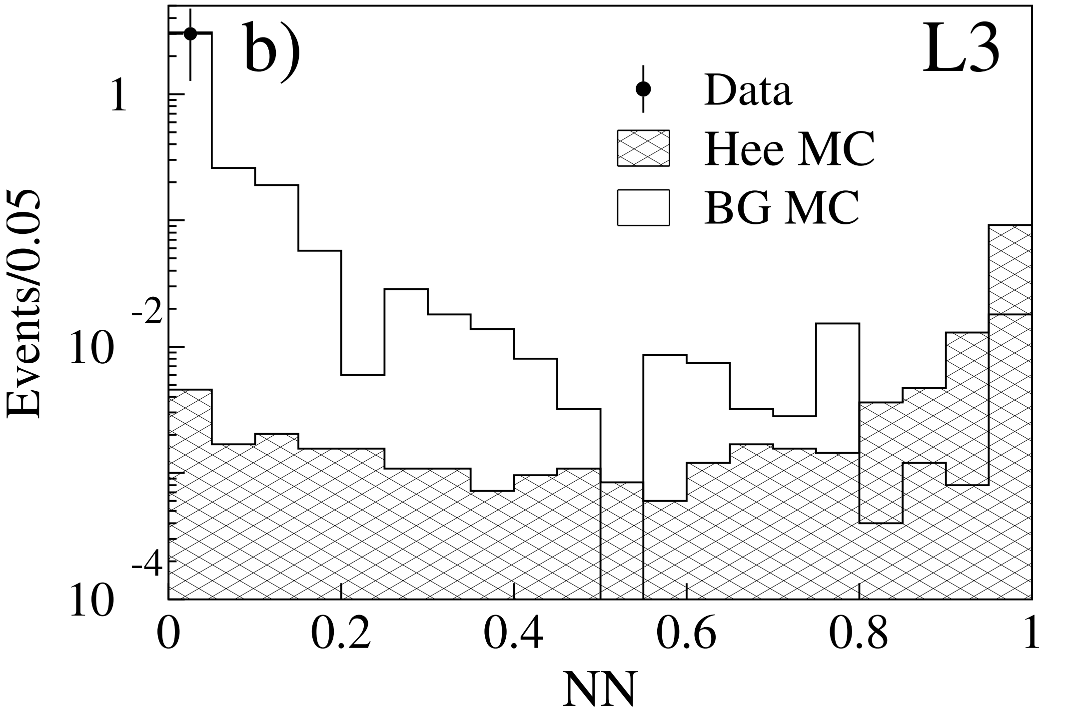

Figure 7: Invariant mass of e^+e^- pairs for the He^+e^- selection (a) and final He^+e^- neural network output spectrum (b) for the $\sqrt{s}$ = 172 GeV data sample. The hatched histograms correspond to the 70 GeV Higgs boson signal normalised to the Standard Model cross-section.

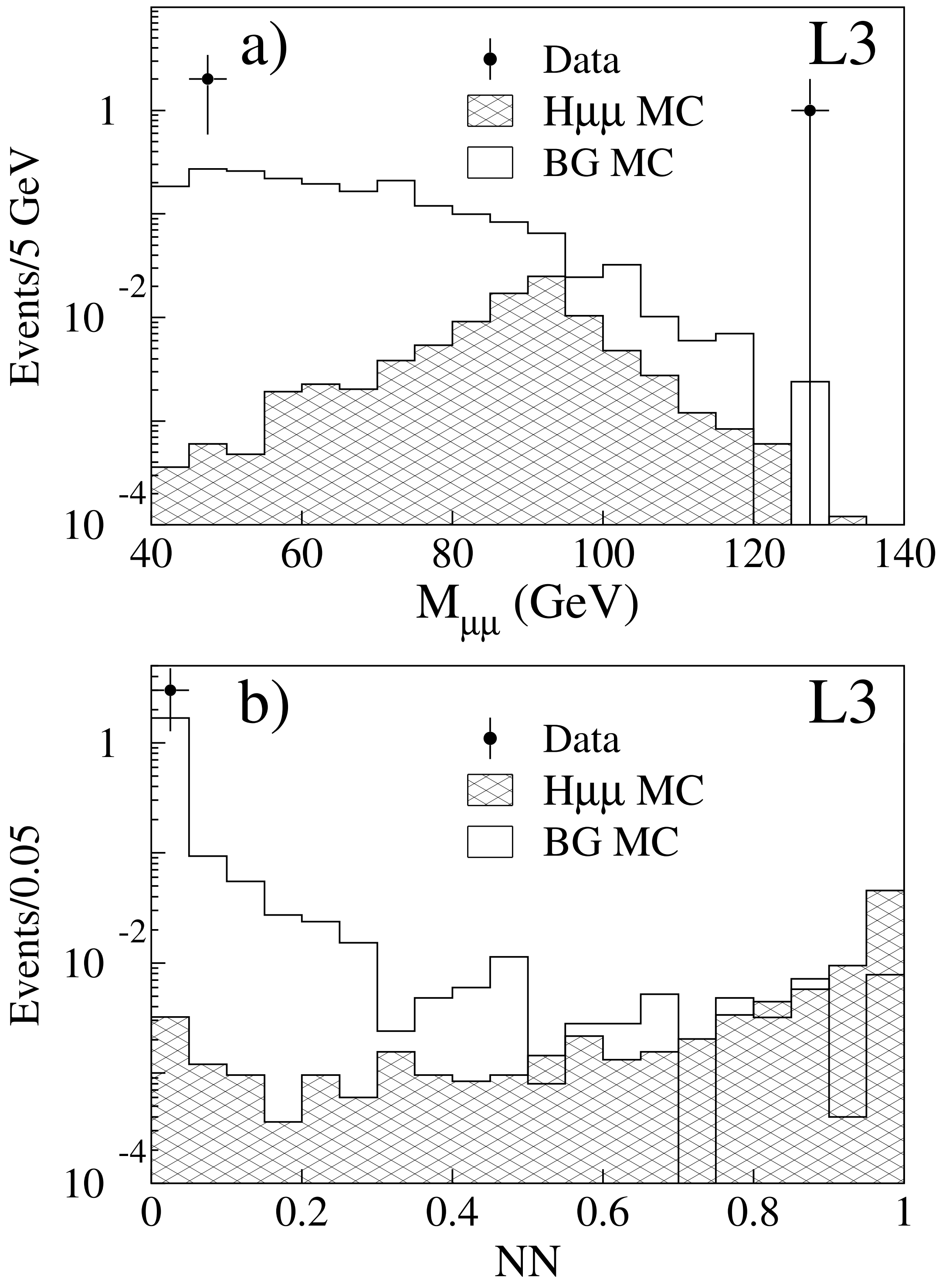

Figure 8: Invariant mass of $\mu^+\mu^-$ pairs for the $H\mu^+\mu^-$ selection (a) and final $H\mu^+\mu^-$ neural network output spectrum (b) for the $\sqrt{s}$ = 172 GeV data sample. The hatched histograms correspond to the 70 GeV Higgs boson signal normalised to the Standard Model cross-section.

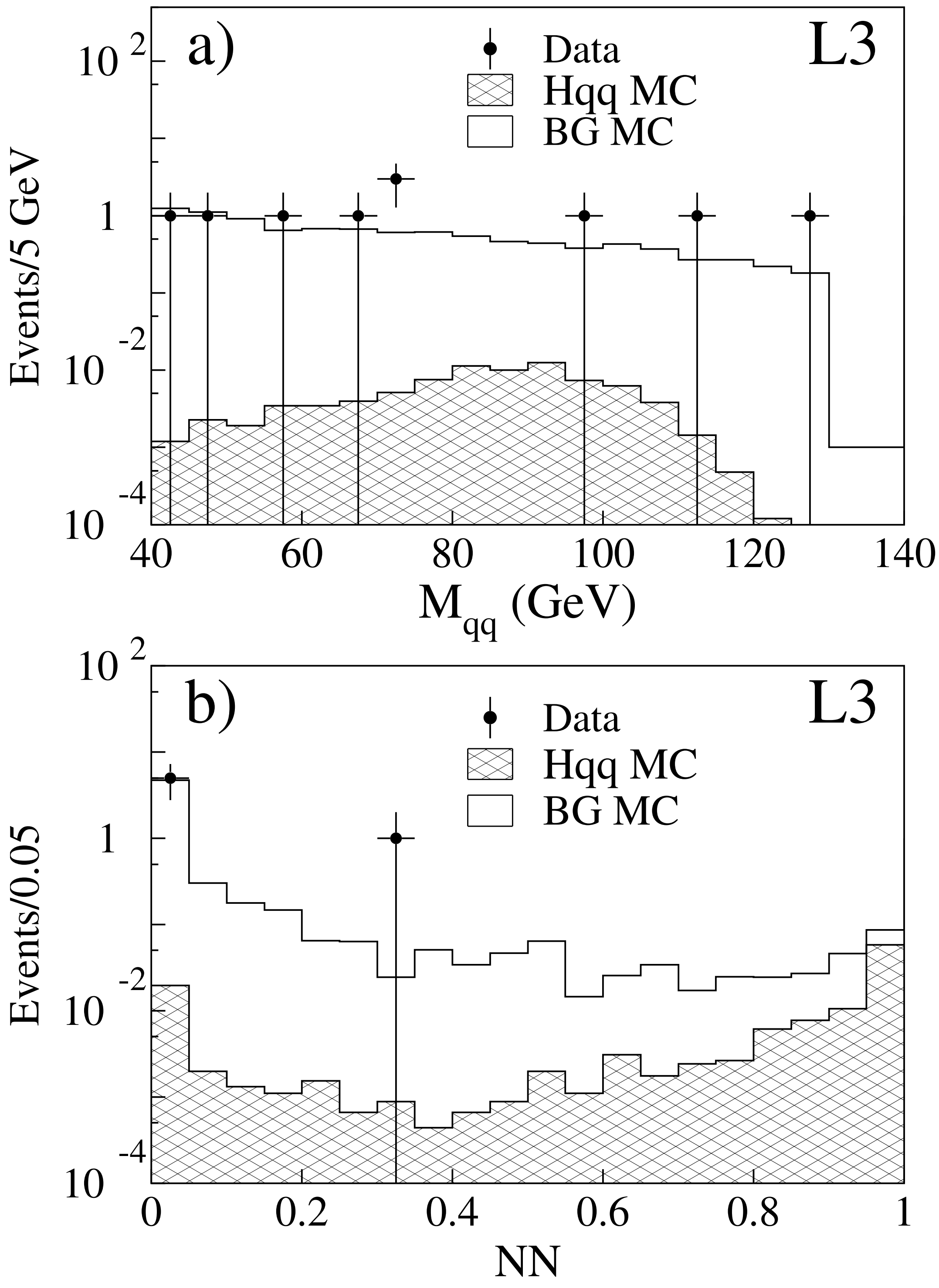

Figure 9: Invariant mass of the hadronic system for the $Hq\bar{q}$, $H \to \tau^+\tau^-$ selection (a) and final $Hq\bar{q}$, $H \to \tau^+\tau^-$ neural network output spectra (b) for the $\sqrt{s} = 172$ GeV data sample. The hatched histograms correspond to the 70 GeV Higgs boson signal normalised to the Standard Model cross-section.

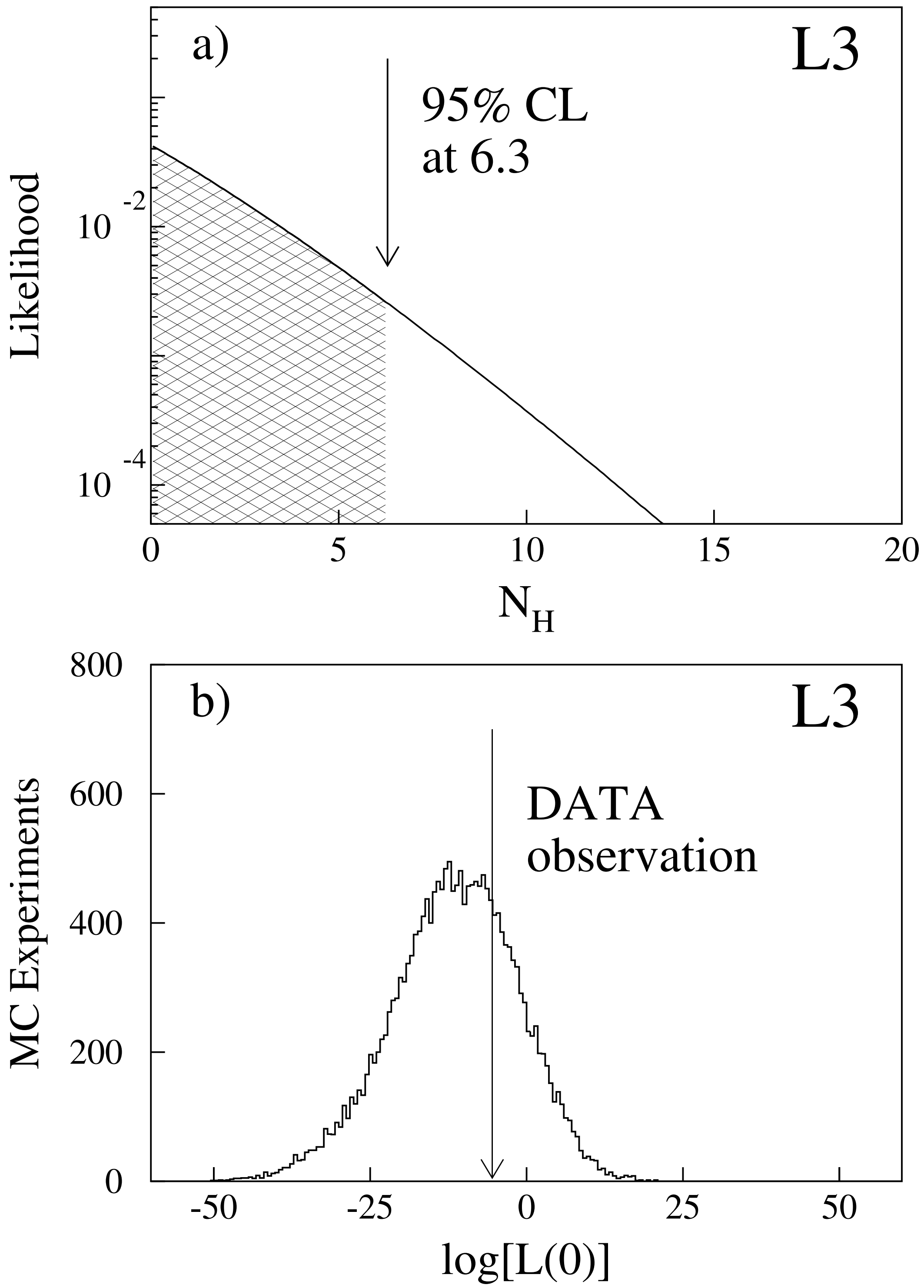

Figure 10: Likelihood function of the number of Higgs signal events representing the outcome of the search(a) and the simulated spectrum of 10000 possible likelihoods for the given background pattern.

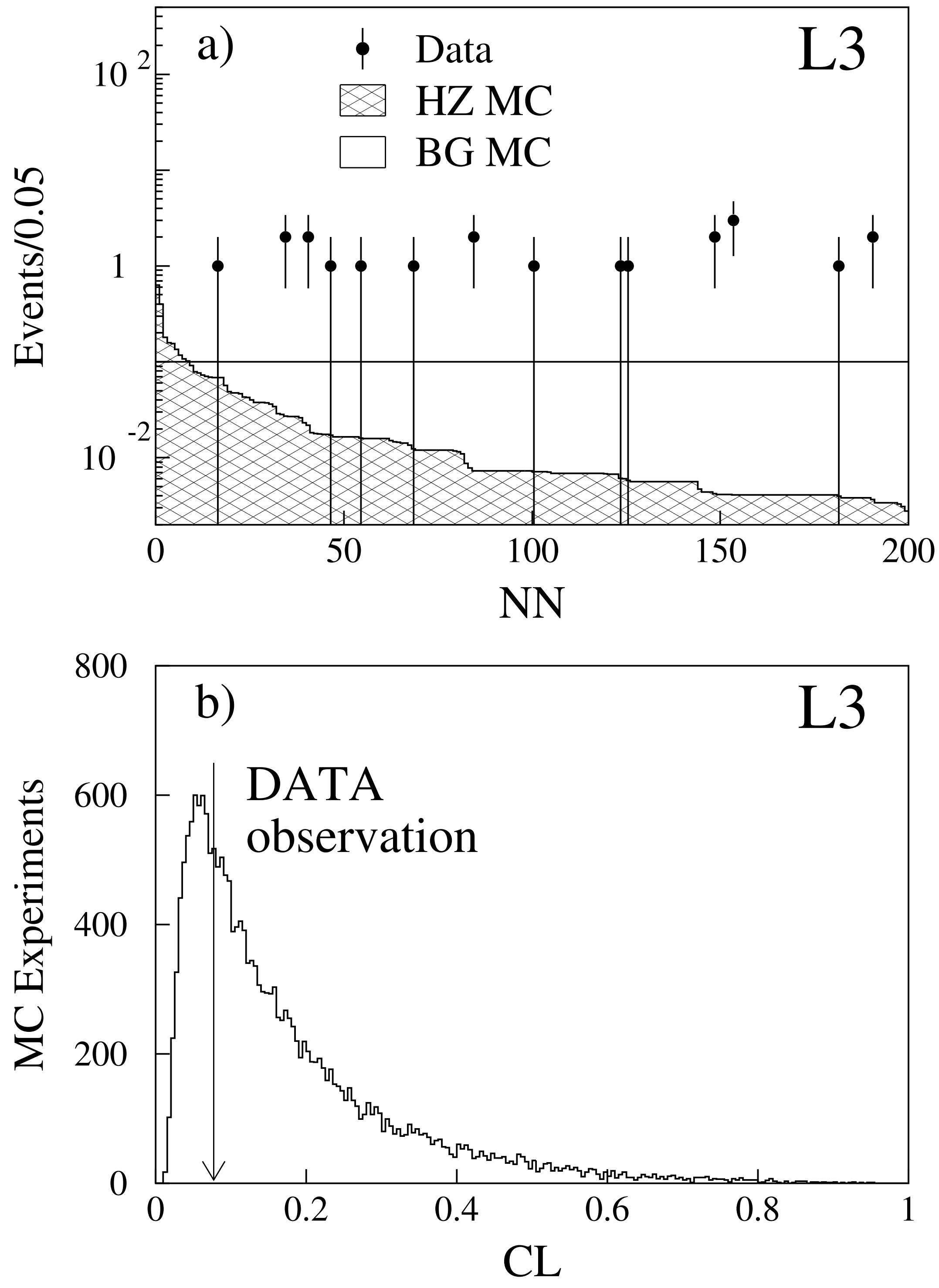

Figure 11: The spectrum of all the neural network output bins for all the channels under ordered according to signal to background ratio (a). The most signal-sensitive region is concentrated near zero. The simulated spectrum of 10000 possible confidence levels for the given background pattern. The confidence level obtained in the present analysis is indicated by the arrow.

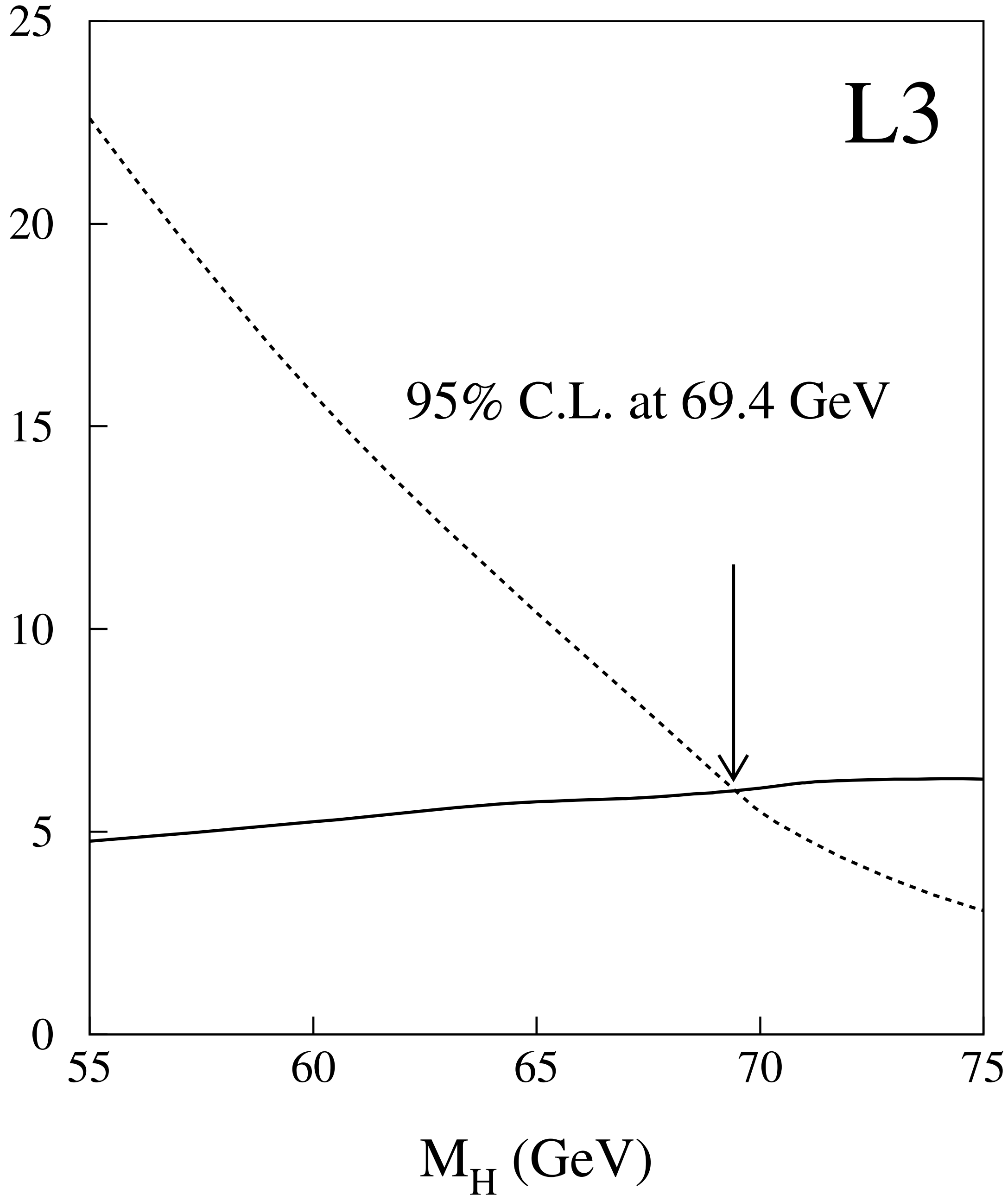

Figure 12: The number of expected Higgs signal events (dashed line) and the number of signal events excluded at 95% confidence level as functions of the Higgs boson mass.